Development of a multifunctional panel for aerospace use through SLM Additive Manufacturing

Available online at www.sciencedirect.com

ScienceDirect

Procedia CIRP 67 (2018) 215 – 220

www.elsevier.com/locate/procedia

11th CIRP Conference on Intelligent Computation in Manufacturing Engineering, CIRP ICME '17

Development of a multifunctional panel for aerospace use through SLM additive manufacturing

Michele Bici[a], Salvatore Brischetto[b], Francesca Campana[a], Carlo Giovanni Ferro[*,b], Carlo Seclì[c], Sara Varetti[b,d], Paolo Maggiore[b], Andrea Mazza[b]

[a] *Sapienza Università di Roma, Via Eudossiana 18, 00184 Roma*
[b] *Politecnico Di Torino, Corso Duca degli Abruzzi 24, 10129 Torino*
[c] *Altair Engineering, Via Livorno 60, 10144 Torino*
[d] *3D- New Technologies (3D-NT), via Livorno 60, 10144, Torino*

* Corresponding author. Tel.: 011.090.68.58; *E-mail address:* carlo.ferro@polito.it

Abstract

Lattice materials can overcome the need of light and stiff structures in the aerospace industry. The wing leading edge is one of the most critical parts for both on-board subsystem and structure features: it must withstand to the aerodynamic loads and bird-strike, integrating also the anti-ice system functions. Nowadays, this part is made by different components bonded together such as external skin, internal passageways, and feeding tubes. In the present work, a single-piece multifunctional panel made by additive manufacturing will be developed. Optimal design and manufacturing are discussed according to technological constraints, aeronautical performances and sustainability.

Peer-review under responsibility of the scientific committee of the 11th CIRP Conference on Intelligent Computation in Manufacturing Engineering

Keywords: DOE; Metamodeling; Pareto optimality; Virtual protyping; Response surface; Additive manufacturing.

1. Introduction

Thermal anti ice is one of the most widely used groups of anti-ice systems and have been extensively used for the anti-icing since the advent of turbomachines [1]. Those systems are installed in the leading edges of airplane to avoid the formation of ice during flight. From theoretical point of view, icing problem on aircraft or on wind turbine has been widely studied [2,3,4,5,6]. An example of P180 [7] aircraft scheme of this system is reported in Fig.1. Insufflating hot air behind the external panels (such as leading edges of wing helicopters blade) assure that the outer surfaces remain at a temperature over ice formation point [8]. Those systems fulfil a vital function: ice forming may cause an overweight on the wing or lock the control surfaces with potential catastrophic effects [9,10,11].
Other kind of anti-ices have emerged as powerful platforms: over the literature is frequent to find proposal of novel piezo electrical anti ice embedded in carbon fiber structures [12,13] or microwave heating sources [14].

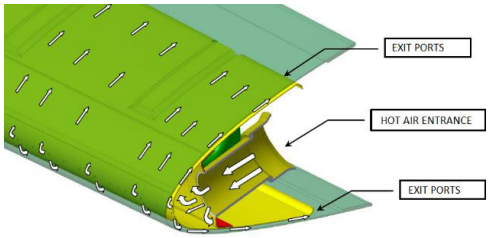

Fig. 1. Layout of P180 anti-ice system [7].

Recently, evidence of flying aircraft, such as the 787, suggests that more electrical airplanes will install more frequently combined power sources. By the way, one of the main obstacles of that type of system is the great current that have to be generated, which would require a revision of the generation system of electrical power. Electro thermal anti ice system is also associated with an increased risk of parasite current and lightning risks.

Peer-review under responsibility of the scientific committee of the 11th CIRP Conference on Intelligent Computation in Manufacturing Engineering
doi:10.1016/j.procir.2017.12.202

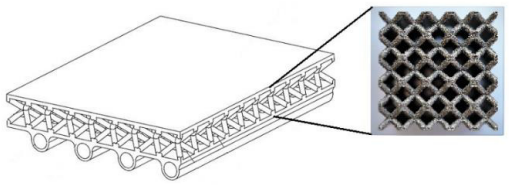

Fig. 2. Panel section with focus on trabecular core.

Despite of it, there is little published data on novel thermal anti ice: most of the papers published have not dealt with the integration of thermal anti ice system inside of the primary structures. The entire system is designed as multiple parts added to the primary structure with joining, bolts or rivets. This work traces the development of a novel system of anti-ice, directly integrated inside the primary structure. This new-patented system [15] uses a lattice core as a heat exchanger, as reported schematically in Fig.2.

Using this sandwich is possible to obtain a light and stiff structure with a great internal thermal exchange surface. Although this novel solution should be complicated to be constructed and tested with traditional technologies, it is easy to be manufactured in a *single-piece* with Additive Manufacturing technology. In fact, Selective Laser Melting (SLM) and Electron Beam Melting (EBM) can realize non-stochastic structures with controlled porosity.

Several papers describe the behaviour of such structures using different material and different cell types, among others [16,17]. The specific objective of this paper is to test different models of cells type and different skin thicknesses to understand which design variable affect mainly the mechanical behaviour.

Data for this study were collected using an aerodynamic 2D CFD tool, Xfoil [18], and a high-fidelity FEM structural code, Optistruct. DOE approach has been utilized introducing Hyper Study to speed up the analysis process. Due to practical constraint, this paper cannot provide a comprehensive view of all the aero-elastic behaviour but is intended to provide new insights for further development.

2. Material and Method

2.1. Model set-up

To establish whether of the design variable affects majorly the mechanical resistance of the sandwich panel, a Design of Experiment (DOE) has been designed. DOE method has been applied through FEM simulations on a NACA profile, using real loads from aerodynamic simulations. FEM model considers the outer skins modelled as shells and the lattice core made by beams. So that, DOE design variables considered in the present work are:

- Cell type: from simple body centered (BCC) to body centered plus vertical beams (BCCZ), as analyzed previously in [19], reported in Fig. 3.
- Cell length: considering thermo-fluid requirements two cell length had been imposed, of 5 and 7 mm each.
- Beam section radius.
- Shell thickness.

FEM geometry (cell type and length) was set-up through a MATLAB code designed for automatize the FEM pre-processing as described in Fig 4.

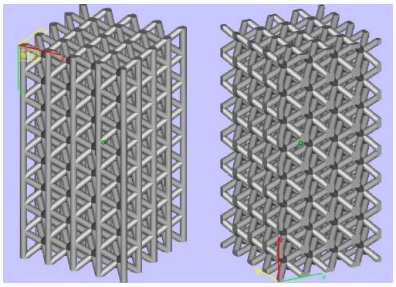

Fig. 3. Cells type made with SLS, on the left BCCZ on the right BCC.

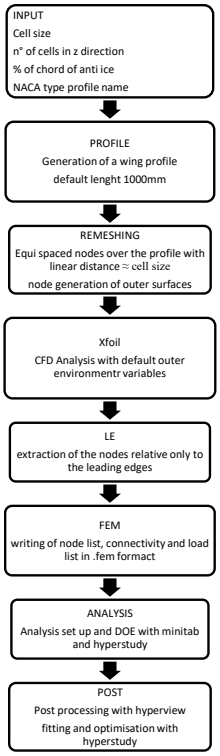

Fig. 4. Set up routine.

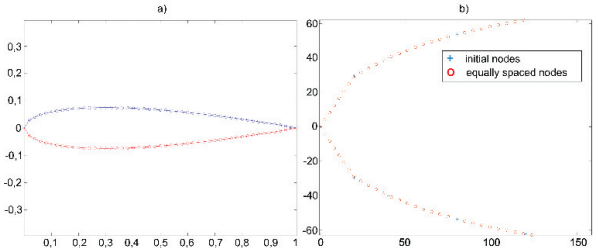

Fig. 5. (a) NACA 0015 profile with un-evenly spaced nodes; (b) original nodes and evenly spaced nodes for the same profile.

The first step in this process was to declare the INPUT request in a series of variable, such as NACA profile type, profile chord length, cell size and number of layers to build in z direction. The process reads this input file and automatically generates a NACA profile with points unevenly spaced along the airfoil. An example of NACA 0015 is reported in Fig.5a. This profile will be the one of the internal skin of the sandwich panel.
After the generation of the sample profile, a remeshing phase generates new nodes evenly spaced along the airfoil, with distance equal to the cell length imposed before, as it can be seen in Fig. 5b. Once the real nodes are created also the internal one and the external projection of the outer skin are generated in this routine.
Imposed the external nodes, it is possible to execute *Xfoil* and to extrapolate the pressure coefficient for each node having the simulation environment fixed as reported in Table 1.

Table 1. Imposed simulation conditions

Name	Value	Unit of Measure
Dynamic Viscosity	0.0000176	Pa s
Air Density	1.1117	kg/m^3
Pressures	898	Pa
Altitude	1000	m
Sound Speed	336.44	m/s
Velocity	242	km/h
Mach Number	0.3	---
Reynolds Number	450000	---

The simulation environment reflects the condition of a medium size liner airplane or UAV HALE during climbing phase at 1000 metres of altitude at a true speed of 242 km/h. The selection of this condition represents a real icing condition where the system could be activated.

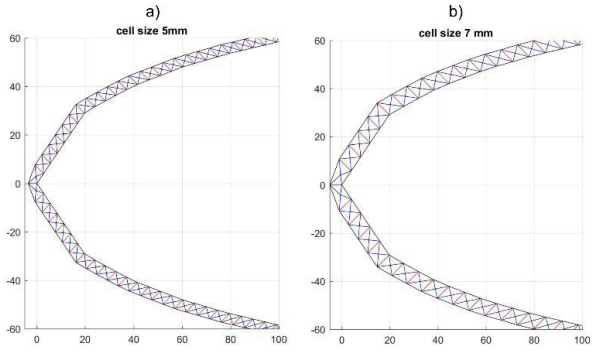

Fig. 6. (a) Leading edge panel with 5mm length; (b) Leading edge panel with 7mm length.

The final stage of the MATLAB routine is writing in normalized format of the node list, the connectivity of the entire panel and the load applied. It is important to remark that, for the purpose of this work, only the leading edges were selected (skimmed as a percentage of the chord length). Fig. 6 represents a view of the two panel with different cell size.
The FEM analysis have been performed over a portion of the entire profile relative to the leading edges, approximately at 50mm of chord length. Due to cell constraint, the length of the two panels cannot be exactly of the length same.
Structural behaviour of the panel was assessed by a linear static analysis and a modal analysis. Load conditions were those related to Table 1 and boundary constraints were imposed to avoid movements outside the plane and to reproduce riveting of the panel with the remaining part of the structure. Structural analysis set-up was made importing the model geometry derived from the MATLAB in Hyperworks17, using Optistruct as solver.

2.2. Doe set up

A DOE (Design of Experiment) was defined to analyse the effect of the lattice-core characteristics (cell type and length) on structural behaviour. For each cell length, the effects of beam-section radius and the shell thickness were investigated by means of a Central Composite Design (CCD), as reported graphically in Fig. 7. It has been chosen to give evidence of linear and non-linear effects, including interactions among variables, also providing reliable response surface models, suitable for design optimization [17].
Table 2 shows the CCD definition applied to beam radius and thickness shell variables. Their values were set in the ranges of 0.35÷0.65 mm and 0.40÷1.00 mm, respectively.

Table 2. Used values of Beam Radius and Shell Thickness in CCD.

Run	*1*	*2*	*3*	*4*	*5*	*6*	*7*	*8*	*9*
Beam Radius (mm)	0.39	0.39	0.61	0.61	0.35	0.65	0.50	0.50	0.50
Shell Thick. (mm)	0.49	0.91	0.49	0.91	0.70	0.70	0.40	1.00	0.70

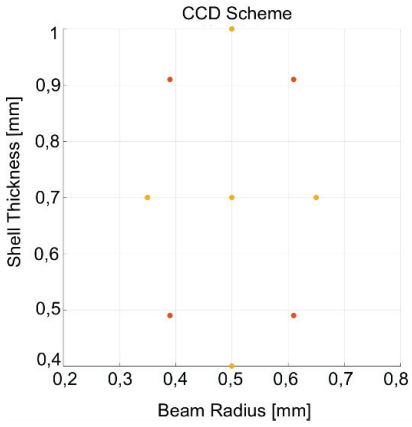

Fig. 7. Scheme for the CCD adopted.

This DOE was replicated for two different cell types, reported in Figure 3:

- Cell_1: body centred plus vertical beams, BCCZ;
- Cell_2: simple body centred, BCC;

and for two cell lengths, selected to take into accounts different heat sections and related thermal constraints that are not considered directly in this work. They are:

- length_7: cell length equal to 7 mm;
- length_5: cell length equal to 5 mm;

The study had involved 36 different simulations divided into four sets, the first group by length and the second by type.

3. Results

In this section, the results obtained from the model set-up of the simulations, both for finding the aerodynamic loads and the structural responses, are presented together with the results achieved by the four sets of DOE.

3.1. Aerodynamics loads

To assess which of the parameter influences majorly the mechanical behaviour aerodynamic load had to be computed. To fulfill this *Xfoil* has been used giving a profile paneling conveniently generated from MATLAB with a spacing equal to the cell length. To avoid the bias in load due to the external augmented thickness of the 7 mm-case a reshaping of that profile has been carried to uniform the section magnitude.

Polar graphs for the two cases are reported in Fig. 8 and 9.

As reported by the graphs, the C_p value has some noises in the trend especially near to the leading edges where presents some spikes. These numerical errors are imputable to the coarse paneling and have been filtered in the post processing phase with MATLAB.

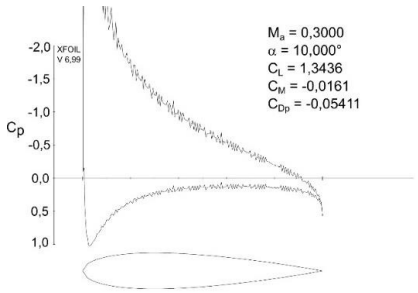

Fig. 8. Polar diagram for 0015 profile with 5 mm paneling.

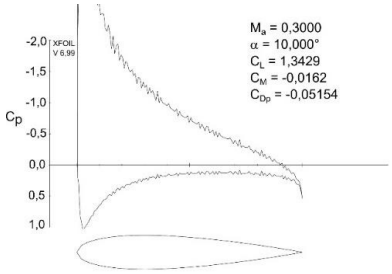

Fig. 9. Polar diagram for 0015 profile with 7 mm paneling.

3.2. Structural FEM analysis

DOE results were taken from FEM analysis, in particular output was managed by Hyperstudy and related to the following FEM responses:

- Maximum beam stress in the vertex of the profile and in the most loaded constraint.
- Maximum displacement and shell stress of the structure, in the middle section of the upper part of the panel.

Figures 10, 11 and 12 shows the contour of these responses highlighting maximum values, comparing the deformed structure to the undeformed one. Fig. 13 shows also the first mode of the modal analysis. It was selected, together with total mass, as the objective functions of the optimization problem faced through the response surface achieved by the DOE.

3.3. DOE results

According to section 3.2, DOE results consist with 6x36 response evaluations, not entirely reported for sake of brevity. Concerning stress responses both length_5 and length_7 has the same behaviour changing beam radius and shell thickness.

Fig. 14 shows beam stress at the vertex, with cell_1 (BCCZ), for the two different cell lengths.

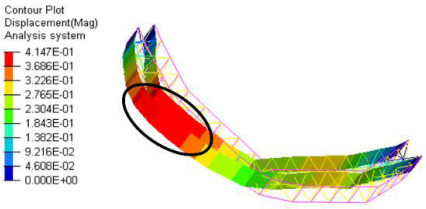

Fig. 10. Example of displacement trend with the maximum displaced zone in the black ellipse

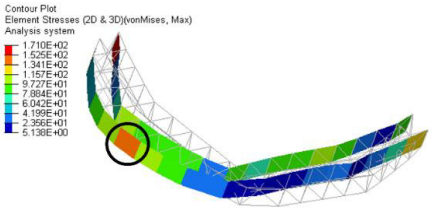

Fig. 11. Example of shell stress trend with the maximum stressed zone in the black circle.

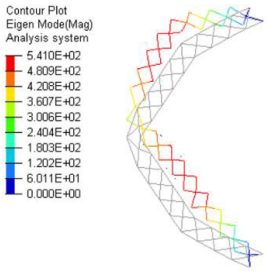

Fig. 12. Example of beam stress trend and the two considered zones: @vertex (red ellipse) and @upper constraint (black ellipse).

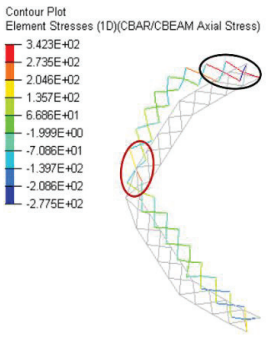

Fig. 13. Example of the deformed shape for the first natural mode.

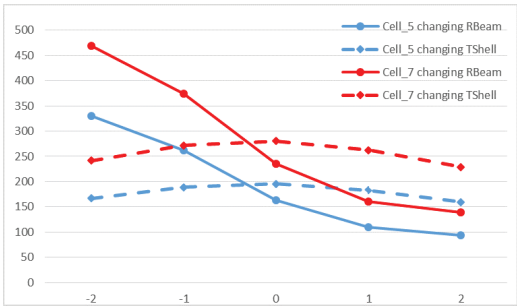

Fig. 14. Beam Stress @Vertex (in MPa) changing R-Beam and T-Shell for the two lengths in cell_1 configuration.

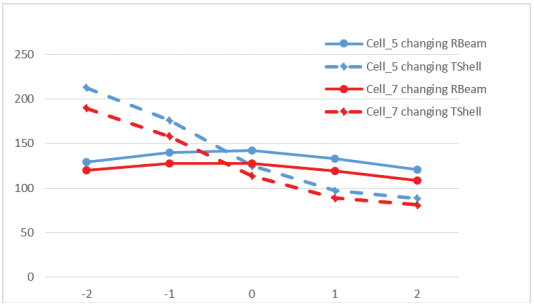

Fig. 15. Maximum Shell Stress (in MPa) changing RBeam and TShell for the two lengths in cell_1 configuration.

Fig. 15, instead, shows the same kind of analysis related to maximum shell stress, obviously highlighting (by a comparison to the Fig. 14) the dependence of beam stress from the Beam Radius and the dependence of the shell stress from the Shell Thickness.

Considering maximum displacement, length_7 provides a minor influence of shell thickness both in case of cell_1 and in case of cell_2. On the contrary, in case of length_5, principal effects of shell thickness and beam radius are quite similar.

We can also observe a decrease of stress passing from the cell_1 type to the cell_2. This can be explained considering that the cell_2 implies a less rigid structure, transforming the given energy (by the loads) more into displacement than into stress compared to the cell_1 case. For an analogous motivation, in cell_2 type, passing from length_7 to length_5 makes the stress increasing, due to the higher number of cells and elements that produce a more rigid structure (with decreasing displacement).

Concerning mass of the structure, length_7 has higher weight than length_5 since although it has more cells length_7 must have longer beams.

Concerning frequency of the first mode, length is the most effective variable, moving the frequency from mean values of 3.7 kHz for the length_7 to mean values of 3.1 kHz for length_5, while other variables are ineffective.

CCD made starting from a full factorial DOE, as the selected one, allows to see interaction among variables. In our case, only frequency is affected by interaction between shell thickness and beam radius.

To obtain optimal discrete values of Beam Radius and Shell Thickness, we decided to use fitting surfaces, in Hyperstudy, for each one of the four-considered case. The variables had been approximated, through a full quadratic least square regression model, with surfaces, which track the trends already described previously. With this method, we found relative errors lower than the 5% between surfaces and DOE discrete values.

These response surfaces are used as input for the optimization algorithm to get the searched optimal values. We used the Global Response Surface Method (GRSM), defining two objectives:

- minimization of mass in order to have the lightest possible structure;
- maximization of the first natural frequency in order to avoid, as much as feasible, possible resonance effects.

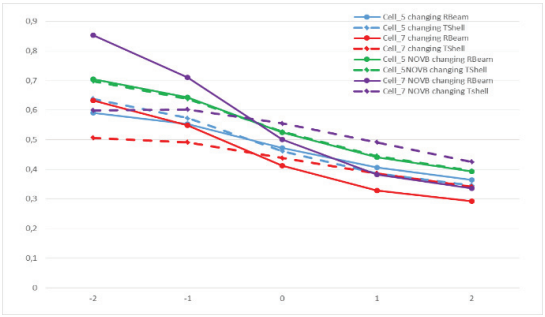

Fig. 16. Maximum Displacement (in mm) changing Rbeam and TShell for the two lengths and the two cell types.

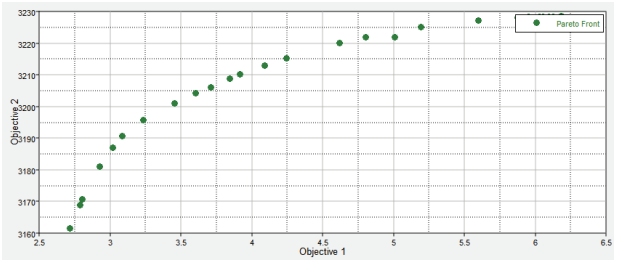

Fig. 17. Example of one of the obtained Pareto fronts.

Table 3. Optimal results.

	Length_5 Cell_1	Length_5 Cell_2	Length_7 Cell_1	Length_7 Cell_2
Beam Radius (mm)	0.350	0.398	0,470	0.496
Shell Thickness (mm)	0.517	0.449	0,400	0.400
Mass (g) (Objective)	3.084	2.836	4,110	3.811
1st Frequency (kHz) (Objective)	3.191	3.154	4,008	3.968
Max Displacement (mm)	0.691	0.772	0,538	0.604
Max Shell Stress (MPa) (Constraint)	172	185	191	180
Max Beam Stress @Vertex (MPa) (Constraint)	329	263	275	230

Also, two constraints had been defined in the optimization. In fact, we decided to control beam (@vertex) and maximum shell stresses, constraining them to stay under 400MPa, considering it a safety threshold since the Yield stress assumed for the considered material (Al7075) about 500MPa.

For each of the considered case (length_5 and length_7 in cell_1 and cell_2 types), we obtained the discrete Pareto fronts, using only the iterations that have respected the constraints (an example is reported in Fig.17). Obtained optimal results are reported in Table 3.

4. Conclusions

In this paper, an innovative solution for a multifunctional sandwich panel was investigated. It consists with a core made by lattice structure and two outer skins, manufactured by additive manufacturing. Aerodynamic loads were investigated by Xfoil and applied to derive simplified FEM models. They were used to understand how cell geometry and structural elements size may affect stress-strain distribution. The analysis was made according to a Central Composite Design (CCD) that analyze beam radius of the lattice core and shell thickness of the outer layers on two different cell types (cell_1 with 12 beams per cell unit and cell_2 with 8) and length (7 mm or 5 mm). Responses investigated maximum stress distribution, total displacement, mass and 1st mode frequency as derived from Optistruct FEM analysis. Beam and shell stresses of cell_1 are higher than that of cell_2 due to a stiffer structure, and comparable results are achieved passing from length_7 to length_5. On stresses, beam radius has the most relevant influence, that in the range decreases non-linearly. Shell thickness has minor effects, parabolic in the range. Only frequency of the 1st mode has interaction effects between beam radius and shell thickness.

The adopted DOE allowed to build a full quadratic response surface that was used to optimize mass and frequency, leaving the maximum stresses under a threshold safe for yielding. From the Pareto frontier of the problem, optimal solutions were evaluated. To optimise mass and 1st frequency beam radius can be set between 0.35 and 0.40 passing from cell_1 to cell_2_ in case of length_5, from 0.47 to 0.50 in case of length_7. Shell thickness, with the same type of progression, changed from 0.52 to 0.40.

In the next future, a multi-disciplinary optimization of the lattice core will be introduced using extensive CFD methods and lumped parameters to evaluate not only the mechanical behaviours but also the thermal dynamic properties during exercise and under deformations. At the end of the analysis campaign, a real demonstrator will be build and tested in a wind tunnel facility with temperature and humidity controls to verify the effectiveness of the patented system.

References

[1] Federal Aviation Administration. Aircraft Icing Handbook. FAA, 1991.
[2] Cao Y., Wu Z., Su Y. and Xu Z. Aircraft flight characteristics in icing conditions. Progress in Aerospace Sciences, 2015, Vol. 74, pp. 62-80.
[3] Xin L., Junqiang B., Jun H., Kun W. and Yang Z. A spongy icing model for aircraft icing. Chinese Journal of Aeronautics, 2014, Vol. 27, pp. 40-51.
[4] Srensen K. L., Blanke M., Johansen T. A. Diagnosis of Wing Icing Through Lift and Drag Coefficient Change Detection for Small Unmanned Aircraft. IFAC-Papers OnLine, 2015, Vol. 48, pp. 541-546.
[5] Politovich, M. K. AVIATION METEOROLOGY: Aircraft Icing. Encyclopedia of Atmospheric Sciences. 2015.
[6] Parent O., Ilinca A. Anti-icing and de-icing techniques for wind turbines: Critical review. Cold Regions Science and Technology, 2011, Vol. 65, pp. 88-96.
[7] Vacca, A. P.180 main wing anti-ice system: analysis and improvements. Genova : s.n., 2013.
[8] MIL-A-9482, Federal Aviation Administration. Anti-Icing Equipment for Aircraft, Heated Surface Type, General Specification. s.l. : FAA.
[9] Bureau d'Enquêtes et d'Analyses pour la sécurité de l'aviation. Final report on the accident on 1st June 2009 to the Airbus A330-203 registered F-GZCP operated by Air France flight AF 447 Rio de Janeiro– Paris. s.l. : BEA, 2012.
[10] Canada, Transportation Safety Board of. Final report on the Transportation Safety Board of Canada's investigation into the accident involving an Air Canada Flight 646 Regional Jet at Fredericton, New Brunswick, on the night of 16 December 1997. s.l. : TSBC, 1999.
[11] NTSA. Aircraft Accident Report, Monday 31 October 1994. 1996.
[12] Tenebre P., Six M. F. Anti icing/De-icing system and method and aircraft structure incorporating this system. US8146866B2 US, April 3, 2012.
[13] Rutherford, R. De ice and Anti Ice system and method for aircraft surfaces. US6194685B1 US, July 30, 1999.
[14] Inoue, N. Anti icing system,wing, aircraft and anti icing method. JP20011/080044 Japan, December 2011.
[15] Ferro C. G., Varetti S., Vitti F., Maggiore P. An aircraft equipped with astructurally integrated de-icing system. IT102016000098196 September 2016.
[16] Yan C., Hao L., Hussein A., Young P., Huang J., Zhu W. Microstructure and mechanical properties of aluminium alloy cellular lattice structures manufactured by direct metal laser sintering. Materials Science and Engineering A, 2015, Vol. 628, pp. 238-246.
[17] Yan C., Hao L., Hussein A., Bubb S. L., Young P., Raymont D. Evaluation of light weight AlSi10Mg periodic cellular lattice structures fabricated via directmetal laser sintering. Journal of Materials Processing Technology, 2014, Vol. 214.
[18] Drela M., MIT. http://web.mit.edu/drela/Public/web/xfoil/. [Online] [Cited: June 01, 2017.]
[19] Varetti, S. Design and characterization of trabecular structures of aluminum alloy produced by DMLM (Direct Metal Laser Melting) for aeronautical sandwich panels. Turin : s.n., 2016.
[20] Montgomery, D. Design and Analysis of Experiments. John wiley & sons, 1997. ISBN 0-471-31649-0 .
[21] Altair. HyperStudy User Guide. 2017.